Fallback Options for Airgap Sensor Fault of an Electromagnetic Suspension System

Konstantinos Michail[a], Argyrios C. Zolotas[b], Roger M. Goodall[c]

[a]*Department of Mechanical Engineering and Materials Science and Engineering, Cyprus University of Technology, Limassol, Cyprus (e-mail: kon_michael@ieee.org)*
[b]*School of Engineering and Informatics, University of Sussex, United Kingdom (e-mail: a.zolotas@sussex.ac.uk)*
[c]*Control Systems Group, School of Electronic, Electrical and Systems Engineering, Loughborough University, United Kingdom (e-mail: r.m.goodall@lboro.ac.uk)*

Abstract

The paper presents a method to recover the performance of an electromagnetic suspension under faulty airgap sensor. The proposed control scheme is a combination of classical control loops, a Kalman Estimator and analytical redundancy (for the airgap signal). In this way redundant airgap sensors are not essential for reliable operation of this system. When the airgap sensor fails the required signal is recovered using a combination of a Kalman estimator and analytical redundancy. The performance of the suspension is optimised using genetic algorithms and some preliminary robustness issues to load and operating airgap variations are discussed. Simulations on a realistic model of such type of suspension illustrate the efficacy of the proposed sensor tolerant control method.

Keywords: Maglev, Active suspensions, Airgap sensor fault, Kalman estimator, Genetic Algorithms

1. Introduction

MAGnetic LEVitation (MAGLEV) trains have been attractive to the transport industry due to a number of advantages they offer compared to conventional wheel-on-rail equivalents. In particular, MAGLEV trains have no mechanical contacts with the rail thus reducing maintenance costs, although in general building MAGLEV rail infrastructure is more expensive than conventional rail infrastructure [18].

MAGLEV suspensions offer high performance with desirable levels of ride quality, they are inherently unstable systems thus stabilised by appropriate control solutions while they can be very sensitive to sensor faults with high probability of instability developing under such failures. MAGLEV suspensions are typically separated into two types. One is the **E**lectro-**D**ynamic **S**uspension and the second, which is considered in this paper, is the **E**lectro-**M**agnetic **S**uspension (EMS). If the EMS system becomes unstable it can either fall off or stick to the rail causing series of undesirable effects to the train and its passengers. Hence, being a critical-safety system substantially increases costs as it is requires a **F**ault **T**olerant **C**ontrol (FTC) structure [3]. Typically, two types of FTC exits [23], one is the *passive* type where the controller is designed to be insensitive to faults, while the second type, the *active* where the controller changes structure (sort of remedial action or reconfiguration) when a fault occurs [16, 29]. Safety-critical systems employ either active or a combination of active-passive FTC.

Previous studies on active fault tolerant control for EMS systems aimed to increase the reliability while keeping hardware redundancy to a minimum. Work from other authors related to detect and accommodate

sensor faults, controller or even electromagnet failures, i.e. (i) state feedback control where the authors targeted recovering from current or acceleration sensor failures [15], (ii) fault tolerant control using classical PID with tracking differentiators for acceleration sensor failure[31], (iii) LMI-based H_∞ approach where the authors aimed to recover from airgap or accelerometer sensor faults as well as accommodate actuator (electromagnet) faults [26], (iv) simultaneous stabilisation-based fault tolerant control against electromagnet failures is also considered in [30], (v) sensor fault diagnosis using a bank of Kalman estimators has been considered for detection and location of sensor faults in [28] and (vi) redundant controllers to offer some form of hardware redundancy [17, 19] for possible controller failures.

The particular contribution of this paper lies in a fault tolerant control approach aiming to reduce hardware sensor redundancy while maintaining appropriate maglev suspensions performance for both deterministic and stochastic inputs under parametric uncertainties. In particular, the paper extends concepts presented in [9] and [11] as well as airgap estimation using **K**alman **E**stimator (KE) attempting to offer simplicity in the solutions, i.e. minimize airgap sensor redundancy (noting that airgap measurement is a compulsory element in the control of a maglev suspension, [21]) while avoiding the need for controller reconfiguration by estimating/calculating equivalent airgap information via low cost sensors. The methodology utilises a combination of robust classical control with inner loop control, a KE and complementary analytical airgap signal calculation via alternative low cost sensors. The proposed approach has the advantage of avoiding multiple instances of airgap sensor equipment (i.e. minimise cost), taking in account that airgap sensors are rather expensive in maglev train suspensions. A similar approach, but for a ship propulsion system is seen in [27] for estimating the pitch and the shaft speed under sensor faults, however the authors did not consider the issue of sensor configuration.

Effective control of the maglev suspension requires satisfying a number of control constraints while ensuring acceptable passenger's comfort (stochastic response) and that the vehicle follows rail gradients (deterministic response). Clearly, this is a multiobjective constrained optimisation problem with complex specifications to achieve where evolutionary algorithms can be employed in the tuning of classical-designed controllers and KE for the airgap estimation signal [6]. Although the controllers and Kalman estimator are designed based on the linearised model of the maglev suspension, the control implementation refers to the non-linear model (in order to take in account realistic issues of operating condition).
The performance of the EMS is optimised via **G**enetic **A**lgorithm (GA). Among the different types of GAs the recently developed **N**on-dominated **S**orting **G**enetic **A**lgorithm-II (NSGA-II) based on non-dominated sorting of the individuals in the chromosome [5] is used. NSGAII has very good distribution of solutions on the optimum Pareto front hence it proves to be powerful optimisation tool.

The paper is organised as follows: In Section 2 the linearised quarter car model of the maglev suspension is presented along with possible disturbance inputs to the suspension followed by the control requirements and objectives. Section 3 gives a short description of the genetic algorithm that is used for the performance optimisation. Section 4 explains the proposed optimised fault tolerant control scheme that is based on the combination of classical controllers, kalman estimator. Section 5 illustrates the efficacy of the proposed FTC approach via simulations for 20 sensor fault scenario. Conclusions are included in Section 6.

2. Maglev suspension model and control requirements

The end-view schematic diagram of a MAGLEV vehicle and it's electromagnet suspension system are illustrated in Fig.1. The EMS system represents a one degree of freedom motion, hence labelled as "quarter-car" maglev model. The suspension consists of an electromagnet, with a ferromagnetic core and

a coil which is attracted to the rail that is made out of ferromagnetic material. The mass of the carriage is attached to the electromagnet with z_t being the rail position and z the vehicle position. The difference between the two, $(z_t - z)$ is the airgap. The aim is to control the airgap thus providing appropriate suspension performance to both deterministic and stochastic rail inputs. Assuming that the positive

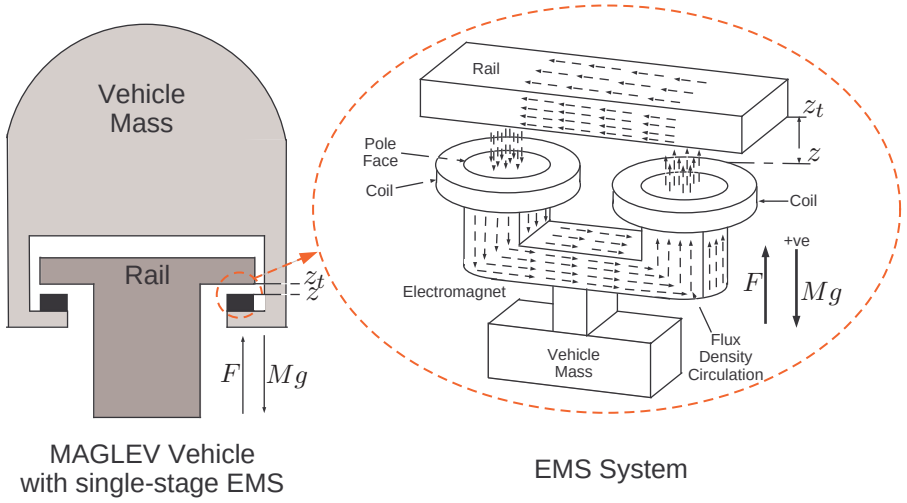

Figure 1: Diagram of a MAGLEV vehicle and the single-stage EMS system.

direction is downwards the equation of motion that stems from Newton's second law is given as

$$M\ddot{Z} = Mg - F \tag{1}$$

Where M is the mass of the carriage, $\ddot{Z}$ is the vertical acceleration of the vehicle, g is the gravity acceleration constant equal to $9.81m/s^2$ and F is the vertical force produced by the electromagnet to maintain the carriage at the operating position.

The electrical circuit of the electromagnet is given by

$$V = RI + L\frac{dI}{dt} + NA\frac{dB}{dt} \tag{2}$$

where, V is the input voltage, R is the coil's resistance, L is the leakage inductance, N the number of turns of the coil and A is the pole face area. I is the coil current and B is the flux density. The linearization takes into account the flux density, the force and the airgap equations in (3) and (4) respectively.

$$B = K_b\frac{I}{G}, \quad F = K_f B^2 \tag{3}$$

$$\frac{dG}{dt} = \frac{dZ_t}{dt} - \frac{dZ}{dt} \tag{4}$$

As indicated by Goodall (2008) [13] the four important variables in the electromagnetic suspension are the force F, the flux density B, the airgap G and the coil current I. The relationships between those variables, are shown in Fig. 2. At constant airgap, the flux density is proportional to the coil current and at constant

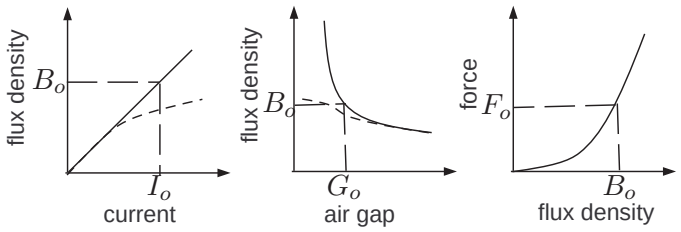

Figure 2: Maglev single-stage suspension non-linearities (Straight lines for theoretical and dotted lines for a practical electromagnet including leakage and saturation).

current is inversely proportional to the airgap. The force is proportional to the square of the flux density. The MAGLEV suspension is non-linear (although no hard nonlinearity appears) but linear controllers can still perform as it is illustrated in Section 5. To derive the LTI state space model, linearisation is done around the operating point using (5)-(7). The 'o' subscript defines the operating point and small letters the perturbation around the operating point. The linerization around the operating point is derived in Michail (2009) [20].

$$F = F_o + f, \qquad B = B_o + b \tag{5}$$

$$I = I_o + i, \quad G = G_o + (z_t - z) \tag{6}$$

$$V = V_o + u \qquad Z = Z_o + z \tag{7}$$

The linearised state-space model of the suspension is given in (8)

$$\begin{aligned} \dot{x} &= A_g x + B_u u + B_{\dot{z}_t} \dot{z}_t \\ y &= C_m x \end{aligned} \tag{8}$$

and the (linear) state vector is: $x = [i, \dot{z}, (z_t - z)]^T$.

The matrices of the state and output equations are given as:

$$A_g = \begin{bmatrix} -\frac{R}{L+K_i NA} & -\frac{K_{(z_t-z)}NA}{L+K_i NA} & 0 \\ \frac{K_b K_i}{M} & 0 & -\frac{K_b K_{(z_t-z)}}{M} \\ 0 & -1 & 0 \end{bmatrix} \tag{9}$$

$$B_u = \begin{bmatrix} \frac{1}{L+K_i NA} \\ 0 \\ 0 \end{bmatrix} \quad B_{\dot{z}_t} = \begin{bmatrix} \frac{K_{(z_t-z)}NA}{L+NAK_i} \\ 0 \\ 1 \end{bmatrix} \tag{10}$$

$$C_m = \begin{bmatrix} 1 & 0 & 0 \\ \frac{K_b}{G_o} & 0 & -\frac{K_b I_o}{G_o^2} \\ 0 & 0 & 1 \\ 0 & 1 & 0 \\ -2K_f \frac{I_o}{MG_o^2} & 0 & 2K_f \frac{I_o^2}{MG_o^3} \end{bmatrix} \tag{11}$$

It is worth noting that the output matrix C_m is shown here to represent all possible measurement quantities, i.e. the current, the flux density, the airgap, and the vertical velocity and acceleration ($[i, b, (z_t - z), \dot{z}, \ddot{z}]^T$). The parameter values for the quarter car model used are given on Table 1. The constants are given as $K_i = B_o/I_o$,$K_{(z_t-z)} = B_o/G_o$ and $K_b = 2F_o/B_o$.

Table 1: Parameters of the EMS system.

Parameter	Value	Parameter	Value
Operating airgap,G_o	0.015m	Carriage Mass,M	$1000kg$
Operating flux density,B_o	1T	Coil's Resistance,R_c	10Ω
Operating current,I_o	10A	Coil's Inductance,L_c	0.1H
Operating voltage,V_o	100V	Number of turns,N_c	2000
Operating force,F_o	9810N	Pole face area,A_p	$0.01m^2$

2.1. Disturbance Inputs and Control Requirements for the Suspension

Two types of disturbance inputs affect the performance of the suspension in the vertical direction. One is of stochastic nature which affect the ride quality of the vehicle and the other is of deterministic which affects the position of the electromagnet on the rail.

2.1.1. Stochastic Inputs

The stochastic input is due to random variations of the rail position as the vehicle moves along the rail. These arise due to rail-laying inaccuracies, steel rail discrepancies as well as due to unevenness during the installation of the rails. Considering the vertical direction, the velocity variations can be approximated by a double-sided power spectrum density (PSD) expressed as:

$$S_{\dot{z}_t} = \pi A_r V_v \tag{12}$$

where V_v is the vehicle speed (taken as $15m/s$ in this case) and A_r represents the roughness and is assigned a value of $1 \times 10^{-7}m$ for high quality rail. The corresponding autocorrelation function is then given as:

$$R(\tau) = 2\pi^2 A_r V_v \delta(\tau) \tag{13}$$

Since a non-linear model is used for the simulations, the rms values of the variables (eg. flux density, coil current etc) are calculated from the values of the time history.

2.1.2. Deterministic input

The main deterministic input to the suspension in the vertical direction comes from the transition onto the rail's gradients. In this work, the deterministic input shown in Fig.3 is used which represents a gradient of 5% at a vehicle speed of $15m/s$, an acceleration of $0.5m/s^2$ and a jerk of $1m/s^3$.

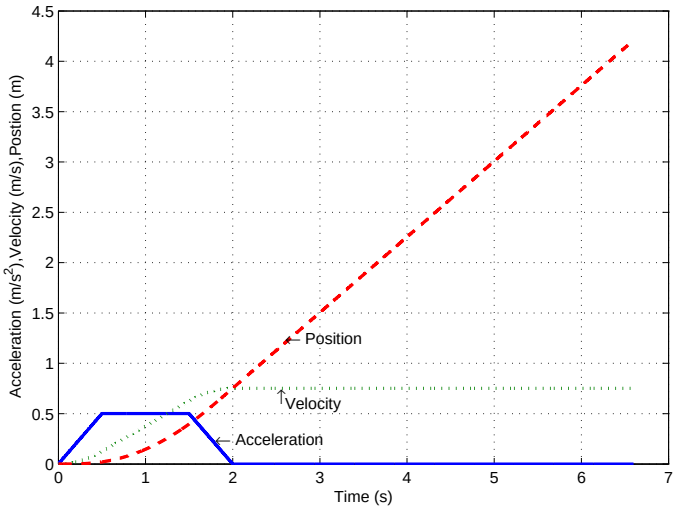

Figure 3: Deterministic input to the suspension with 5% gradient at a vehicle speed of $15ms^{-1}$.

2.1.3. Control design requirements

Fundamentally, there is a trade-off between the deterministic (rail gradient) and the stochastic response (ride quality) of the suspension. For low speed vehicles, performance requirements are described in [10] and [12]. In this paper, the control requirements adhere to the Birmingham MAGLEV vehicle that was operating at Birmingham airport in the United Kingdom for during the nineties [24].

The objective is to minimize both the vertical acceleration, $\ddot{z}$, (improve ride quality) and the excitation of the electromagnets by minimizing the RMS value of the current variations (i_{rms}) about the operating point. Therefore, the objective functions to be minimized are given as:

$$\phi_1 = i_{rms} \quad \phi_2 = \ddot{z}_{rms} \tag{14}$$

Classical control with inner loop flux feedback offers an advantageous approach to controlling a MAGLEV vehicle [11]. Using a Proportional-Integral controller for the inner loop and Phase advance controller for the outer loop, the suspension can perform satisfactorily with sufficient robustness (the latter due to the inner loop). The robustness characteristics come from the frequency response methods as listed on Table 2.

In any real application sensor equipment is affected by noise. For the controlled MAGLEV suspension, noise from sensors can be amplified by the controller and appears on the control signal (the driving signal of the suspension). Particularly, if the controller has high gains, then the amplitude of the noise can become very large. Figure 4 shows the open-loop frequency responses from the control input (u) to the airgap (mm) and also the current (i). It can be seen that the open-loop frequency response has low-pass filter characteristics and therefore the noise is filtered and is expected to have limited effect on the outputs. However, for completeness we introduce a third objective in the optimization to minimize noise effects in the designed system, i.e. (15).

$$\phi_3 = u_{n_{rms}} \tag{15}$$

The required control constraints of the suspension are listed in Table 2.

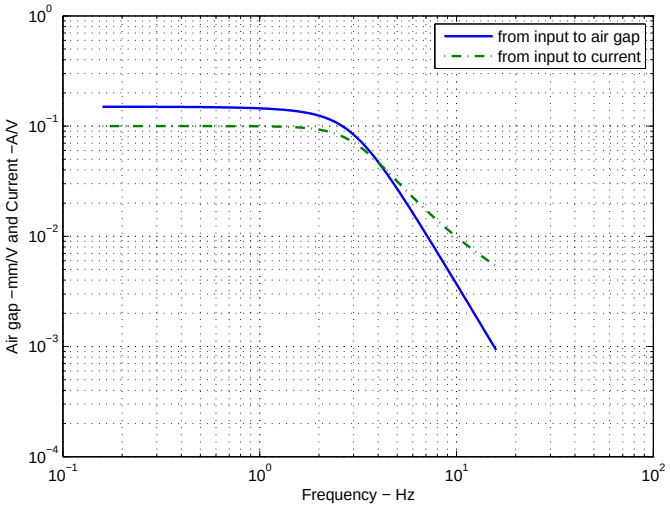

Figure 4: Frequency response from the control input to the airgap/current outputs.

3. Multiobjective constrained optimisation using NSGAII

Genetic Algorithms are heuristic type of optmisation algorithms inspired from nature, see Holland(1975) [14] and introduced by Goldberg(1989) [8]. Since then, GAs have gained serious attention from the scientific community and they have evolved rapidly with a wide range of application in engineering and many other fields taking advantage of their optimisation properties. Among the various versions of GAs, the **N**on-dominated **S**orting **G**enetic **A**lgorithm II (NSGAII) [5] is used in this paper. Optimisation is done in two cases (i) for the optimisation of the classical controllers: The aim of the NSGAII is to find the Pareto-Optimality (i.e. trade-off) between the control objectives (ϕ_1, ϕ_2, ϕ_3) subject to the control constraints listed on Table 2 (eg. both in time and frequency domains). (ii) Kalman-Estimator tuning: In this case, the KE is optimally tuned in order to adequately estimate the redundant airgap signal using the information from the velocity and acceleration sensors.
In order to make sure that the closed-loop control constraints of the suspension listed on Table 2 are satisfied, a constraint handling technique based on penalty function approach is used [4]. An extensive analysis of the NSGAII combined with the penalty functions is given in [22].

The basic parameters used for the NSGAII optimisation process are given next. The crossover probability is generally selected to be large in order to have a good mixing of genetic material. The mutation probability is defined as $1/n_v$, where n_v is the number of variables involved in the optimisation. For the simulated binary crossover parameter (SBX) and the mutation parameter it was decided to use the default values of 20 and 20 since they provide good distribution of solutions for the algorithm operations. Since the NSGAII is used for both the classical controllers and the KE tuning the parameters are different in each case. The number of variables n_v for the classical controller's tuning is five and for the KE only one. The number of chromosomes in the population (P_n) and the maximum generation (G_n) are given for the classical controller tuning, $P_n = 70$ and $G_n = 300$ and for the KE tuning, $P_n = 20$ and $G_n = 70$.

Table 2: Closed-loop Control Constraints Required for the Suspension.

Control Constraints	Value
Stochastic response	
RMS acceleration($\simeq 5\%'g'$),($\ddot{z}_{rms}$)	$\leq 0.5ms^{-2}$
RMS air-gap variation, $(z_t - z)_{rms}$	$\leq 5mm$
Deterministic response	
Max airgap deviation,$(z_t - z)_p$	$\leq 7.5mm$
Control effort,u_p	$\leq 300V(3I_oR_o)$
Settling time,t_s	$\leq 3s$
Frequency response characteristics	
Phase margin,(PM)	$35^o \leq PM \leq 45^o$
Outer bandwidth,$f_{b_{in}}$	$f_{b_{in}}\{^{\leq 100Hz}_{\geq 50Hz}$
Inner bandwidth,$f_{b_{out}}$	$\leq 10Hz$

4. The proposed control scheme for airgap sensor failure

The problem considered in this paper is to recover the performance of the MAGLEV suspension in case of a faulty airgap measurement using redundant still less expensive sensors. The proposed scheme is illustrated on Fig. 5. The suspension has 5 outputs defined in Section 2. Although the control design is based on the linearised model of the EMS, the actual solutions are validated on the nonlinear model [7].

In order to detect a faulty airgap sensor, three airgap signals are compared in between them:

- The measured airgap signal, $(z_t - z)_m$: This signal is the normal measurement as taken from the airgap sensor. It is given directly to the **F**ault **D**etection, **I**solation and **D**ecision **U**nit (FDIDU) as if it passes from a proportional gain equal to one, $K_m = 1$.
- estimated airgap signal, $(z_t - z)_e$: This is the airgap signal as estimated from the KE, K_e, using the velocity and acceleration measurements.
- the calculated airgap signal, $(z_t - z)_c$: This signal is calculated using the current and flux density measurements based on the flux in (3) given as $(z_t - z)_c = K_b \frac{I}{B} - G_o$. This is similar to a proportional gain, K_c, added in the loop.

Additionally, throughout the paper the real airgap signal, $(z_t - z)_r$, is given which is the actual position between the vehicle and the rail i.e. without taking into account airgap sensor dynamics.

Fault Detection and Isolation mechanisms compare the three aforementioned signals and the residuals indicate whether the airgap sensor or one of the other sensors i, b or $\ddot{z}$ are healthy or faulty. In a healthy situation the airgap signal, $(z_t - z)$, is given by

$$(z_t - z) = \left[(z_t - z)_m + (z_t - z)_e + (z_t - z)_c\right]/3 \tag{16}$$

When the airgap sensor is isolated and the airgap signal $(z_t - z)$ is calculated by

$$(z_t - z) = \left[(z_t - z)_c + (z_t - z)_e\right]/2 \tag{17}$$

Consequently, if the calculated or estimated airgap signals are 'faulty', the airgap signal $(z_t - z)$ is calculated accordingly based on (17) using the 'healthy' signals. In order to implement the control scheme of Fig. 5 the classical controllers have to be optimally tuned for optimum[1] performance together with the KE.

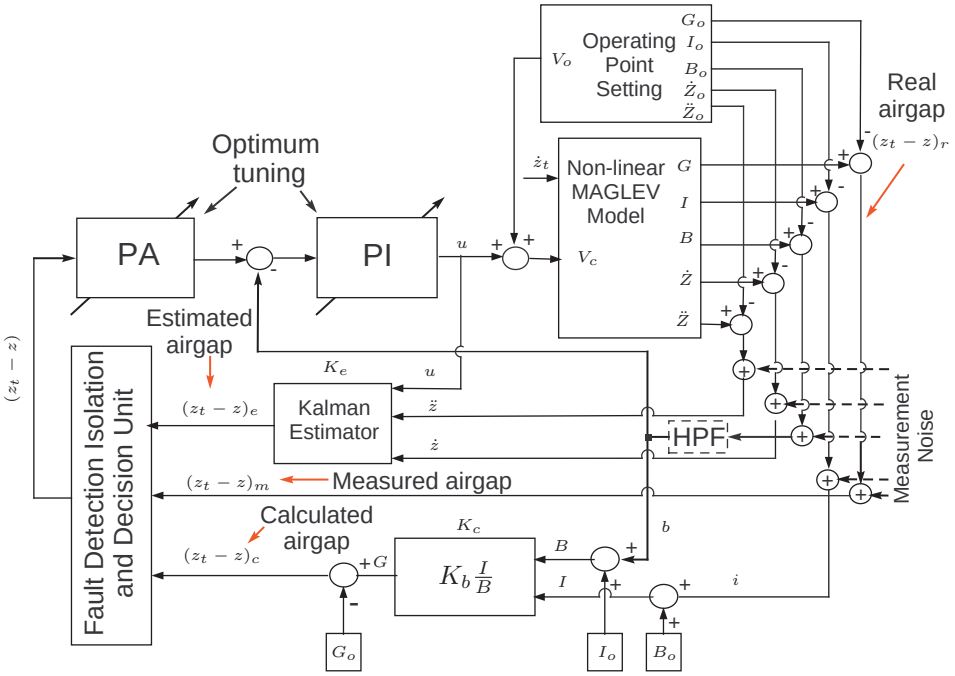

Figure 5: Fallback options for airgap sensor failure of the MAGLEV suspension.

4.1. Sensor Fault Scenarios

A sensor can fail unexpectedly and its behaviour may not be predicted exactly. Faults can be added or multiplied to sensor's output as depicted in Fig. 6, i.e. faults are categorised as additive or multiplicative, with the former been considered here. Given the same figure, faults are separated into three types: (i) abrupt or step-wise fault, (ii) incipient or soft fault and (iii) indeterminate fault.

The performance of the proposed scheme is tested under a number of sensor fault scenaria, with both deterministic and stochastic related simulations. We assume single sensor failure each time. The fault profiles considered fall in the abrupt category both multiplicative and additive type. We consider a total of 5 sensors in the design, i.e. $(i, b, (z_t - z)_m, \dot{z}, \ddot{z})$, each possible to individually fail. An example of the fault introduction (in the deterministic case) can be seen in Figs. 7(a) and 7(b), i.e. the former depicts a multiplicative airgap sensor fault (when fault occurs the sensor amplitude is doubled) while the latter represents an additive fault of random signal profile with very low frequency drift. This type of fault profiles are used for the stochastic response of the suspension and it is assumed to happen on all five sensors. Overall 20 sensor fault tests are considered, with one sensor failing per scenario.

[1]optimum in the sense of "optimized subject to the given constraints" in the application presented in this paper

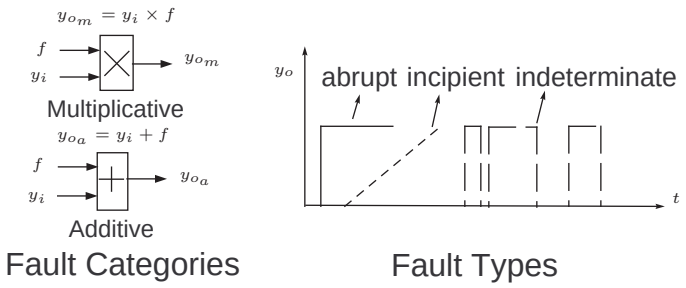

Figure 6: Sensor fault categories and types.

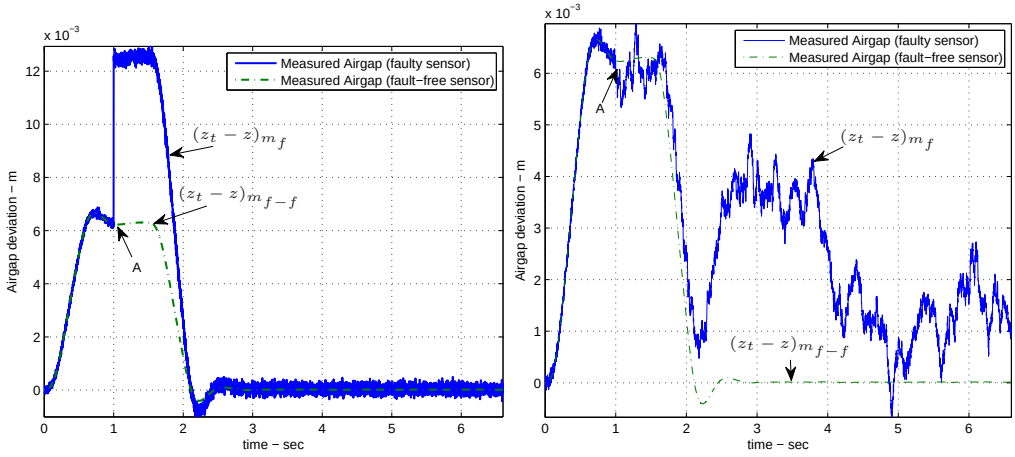

(a) *Multiplicative/abrupt fault profile.* **(b) *Additive/abrupt fault profile.***

Figure 7: Airgap sensor (multiplicative and additive) abrupt fault profiles for a deterministic input to the suspension.

4.2. Classical controller with inner loop design

In order to achieve fault-free optimum performance a similar scheme to the one illustrated in Fig. 5 is used. Particularly, only the airgap ($(z_t - z)_m$) and flux density (b) are fed to the controllers. For the best possible rejection of the disturbance $\dot{z}_t$ and minimisation of the objectives while maintaining suspension performance within safe (see Table 2), the parameters of the controllers are optimally tuned using the NSGAII. The control strategy uses a Proportional-Integral controller (PI) for the inner loop with a bandwidth in the range $50Hz - 100Hz$ while the outer loop is aimed at less than $10Hz$ using the Phase Advance controller (PA). The PA controller in (18), with k the advance ratio and τ the time constant, is used to provide adequate phase margin in the range of $35^o - 45^o$ [11].The controllers' structure are given as

$$PI = G_i \frac{t_i s+1}{t_i s} \qquad PA = G_o \frac{k\tau s+1}{\tau s+1} \tag{18}$$

The controller parameters are tuned simultaneously using the NSGAII and the Pareto-Optimality between the objective functions (ϕ_1, ϕ_2 and ϕ_3) is found accordingly. From those controllers that satisfy the predefined constraints, the desired closed-loop response is selected.

4.3. Kalman Estimator (KE) tuning

The airgap measurement is included as a state in the linearised model of the MAGLEV system (refer to (8)) and therefore a KE can be used estimate it. Note, we consider the design of a continuous-time Kalman estimator.

Consider the following state space expression relating to the linearised MAGLEV model

$$\begin{aligned} \dot{x} &= A_g x + B_u u + B_w \omega_d \\ y &= C_m x + \omega_n \end{aligned} \tag{19}$$

where, ω_d and ω_n are process and measurement noises respectively. These are assumed to be uncorrelated zero-mean Gaussian stochastic processes with constant power spectral densities W and V respectively.

The KE has the structure of an ordinary state-estimator with a state equation as

$$\dot{\hat{x}} = A\hat{x} + Bu + K_f(y - C\hat{x}) \tag{20}$$

where in this case, $A = A_g$, $B = B_u$ and $C = C_m$.

The optimal choice of K_f via W and V is found via minimizing $E\{[x - \hat{x}]^T[x - \hat{x}]\}$ [25]. The optimum choice of W and V eventually control the accuracy of the state estimation. Genetic algorithms are used to tune W in order to minimise the error between the estimated and the measured one for both deterministic and stochastic responses. The noise covariance matrix V is selected to be, diagonal 2×2 matrix with values of the noise covariance for the current and flux density measurements, i.e $V = diag(V_{\dot{z}}, V_{\ddot{z}})$ ($V_{\dot{z}}$ and $V_{\ddot{z}}$ are taken as the square of 1% of the maximum value for the deterministic response). In this design the process noise matrix $B_w = B_{z_t}$ and the process noise covariance matrix W refers to the rail velocity input and this is optimally tuned.

In order to estimate the airgap signal two objectives are selected to minimise via NSGAII. i.e to tune the Kalman estimator presented in (21) and the Integral absolute error between the real airgap and the estimated for both deterministic (ϕ_d) and stochastic (ϕ_s) responses. Although the estimator is stable by default it was important to take the appropriate time domain signal comparison for performance test.

$$\begin{aligned} \phi_d &= \int |(z_t - z)_m - (z_t - z)_e| dt \\ \phi_s &= RMS((z_t - z)_m - (z_t - z)_e) \end{aligned} \tag{21}$$

In this case, it is important to obtain an accurate for the estimate of air-gap and therefore two constraints are assigned so that the related error is less than 5% (22).

$$\begin{aligned} \omega_d &= \int |(z_t - z)_m - (z_t - z)_e| dt \leq 0.05 \\ \omega_s &= RMS((z_t - z)_m - (z_t - z)_e) \leq 0.05 \end{aligned} \tag{22}$$

5. Simulations and data analysis

5.1. Performance optimisation of the EMS

The control strategy with classical approaches was optimally tuned and the desired performance of the MAGLEV suspension has been achieved. Figure 8 depicts the Pareto-Optimality between 2 out of 3 objective functions. Although there are three objectives to be minimized, only the trade-off between the i_{rms}, (ϕ_1) and $\ddot{z}_{rms}$, (ϕ_2) is depicted which is of main interest. A 3D figure is avoided because the trade-off is not clearly shown due to the nature of such plot. The maximum level of the noise, $u_{n_{rms}}$ (ϕ_3)

is restricted to around $25V_{rms}$. This looks fairly high but as explained in Section 2.1.3 the noise is largely reduced from the low-pass filtering properties of the suspension (see Fig. 4).

The vertical acceleration (i.e. ride quality) of the suspension is less than $0.5m/s^2$ while the input current from the stochastic behaviour is limited to around $1A$. From the optimum Pareto front of controllers depicted in Fig. 8 all controllers (each point reflects to one controller) shown are tuned to satisfy all control constraints listed in Table 2 and therefore anyone of them can be selected based on the user's requirements. The pair of controllers (PA,PI) that results in the best ride quality (i.e. smallest $\ddot{z}$) which is given in (23) is selected.

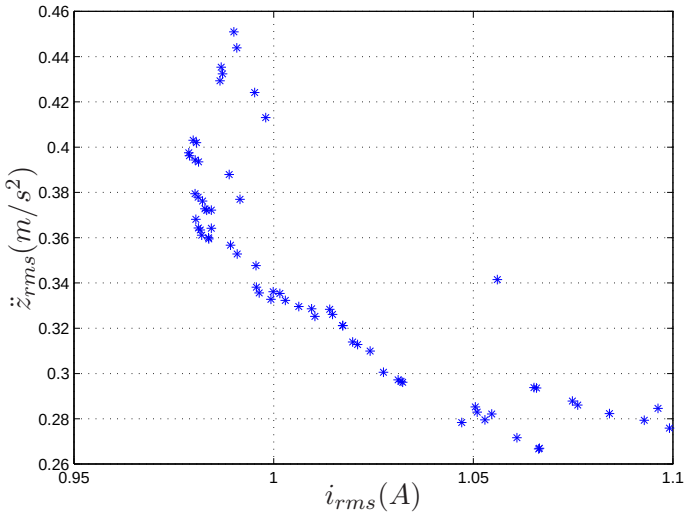

Figure 8: Pareto front of controllers using NSGAII.

$$PA = 3.98\frac{0.1323s+1}{0.0244s+1} \quad PI = 1.1642e3\frac{0.0052s+1}{0.0052s} \tag{23}$$

The resulting vertical acceleration (ride quality) is $0.26m/s^2$ and the airgap deviation for a 5% rail gradient is shown in Fig. 9(a). All the control constraints from the deterministic rail profile are satisfied including maximum airgap deviation and settling time. It is clear that the noise on the input voltage, u in Fig 9(b) does not affect the performance of the suspension and the maximum peak value of u constraint is satisfied. Using the proposed optimisation method, the controllers are successfully tuned and the next stage is to show that the Kalman estimator is able to estimate the airgap signal using the vertical velocity ($\dot{z}$) and the acceleration ($\ddot{z}$) measurements.

5.2. Airgap estimation based on Kalman estimator

The KE has been tuned as explained in Section 4.3 for the airgap signal estimation using both deterministic and stochastic input profiles.
The optimum values for V and W are given in

$$V = diag(5.8537, 3.3301)10^{-5}, W = 3; \tag{24}$$

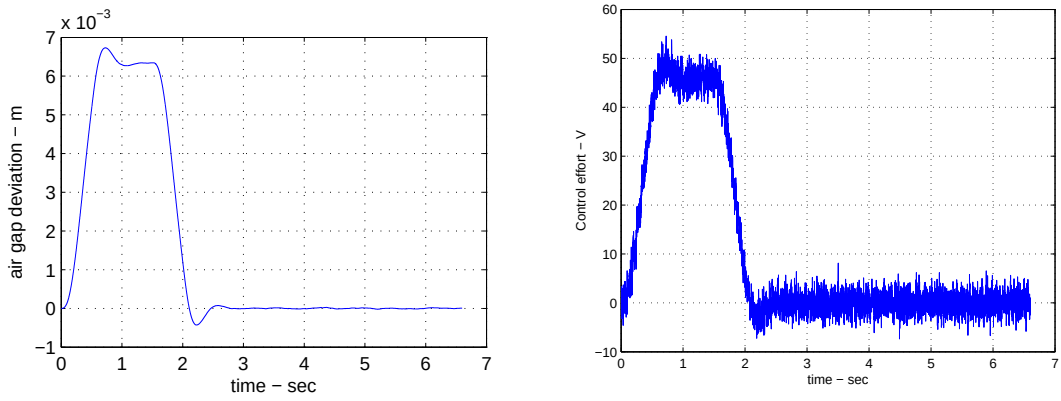

(a) *Real airgap,* $(z_t - z)_r$**.** **(b) *Input voltage,*** u**.**

Figure 9: Real airgap ($(z_t - z)_r$) and input voltage (u_c) from the deterministic rail profile.

and the resulting KE gain is given as

$$K_f = \begin{bmatrix} -0.0689 & -190519.1264 \\ 0.7542 & 1.0044 \\ -0.0005 & -300.1438 \end{bmatrix} \tag{25}$$

Figure 10 shows the error between the different airgap signals involved for the fault detection and decision making unit: Fig. 10(b) the measured and the estimated ($e_{(z_t-z)_{m,e}}$), Fig: 10(a): the measured and calculated ($e_{(z_t-z)_{m,c}}$) and Fig. 10(c): the estimated and calculated airgap signals from the deterministic response of the suspension. Similar results are obtained with the stochastic rail input hence not illustrated here. The errors are fairly small with both disturbance inputs therefore these signals can be used for the fault detection and decision making unit.

5.3. Robustness analysis

The Maglev suspension system performance is subject to some parametric variations in the system including load variation and uncertainty that could occur on the operating point of the airgap, G_0.

5.3.1. Load variations

The suspension has to support the mass of the vehicle as well as the passengers' weight (load). We assume a variation of 25% load, i.e. for quarter vehicle the laden vehicle mass (vehicle+load) increases to 1.25 tonnes. The above variation is quite substantial for the maglev application and the system should maintain adequate performance in such case.

The load variation is simulated in the form of an external disturbance force, i.e. F_d on the mechanical equation part from (1). Note that $F_d = \Delta M * g$, where ΔM is the passengers' mass. We assume a ramp profile (over 10 seconds) of varying load from 0 to 250kg, i.e. 0-250*9.81N. The F_d profile can be seen in Fig. 11(a). The profile depicts passengers boarding the maglev vehicle compartment while the train is stopped at a station (with the vehicle hovering). The assessment is done for the deterministic case (although a similar pattern has been noted in the stochastic one), however it is worth noting that

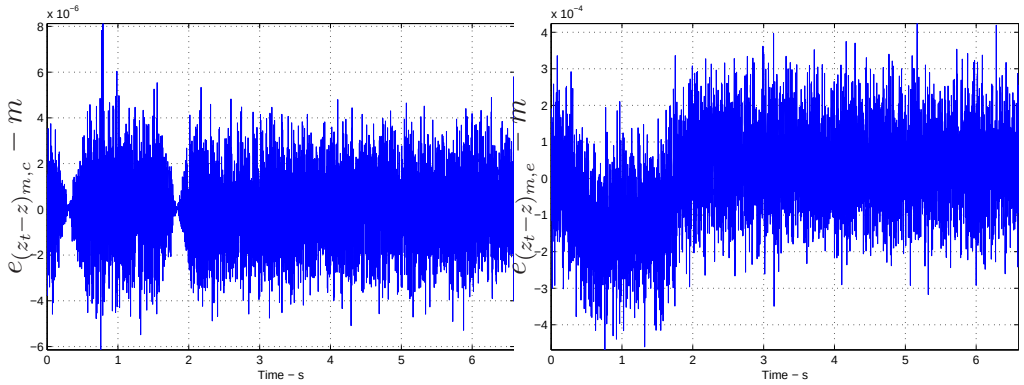

(a) ***Error between measured and calculated airgap,*** $e_{(z_t-z)_{m,c}}$.

(b) ***Error between measured and estimated airgap,*** $e_{(z_t-z)_{m,e}}$.

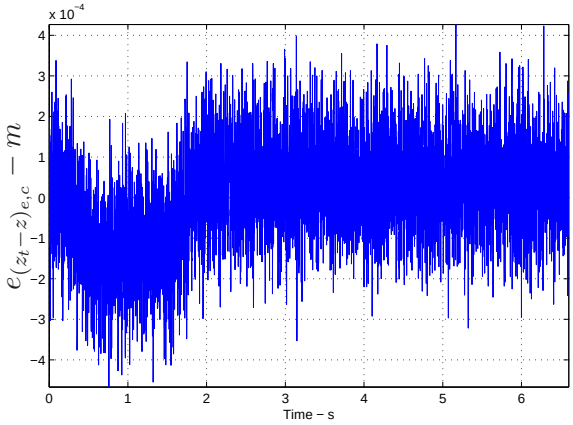

(c) ***Error between estimated and calculated airgap,*** $e_{(z_t-z)_{e,c}}$.

Figure 10: Error between the measured-estimated ($e_{(z_t-z)_{m,e}}$), measured-calculated ($e_{(z_t-z)_{m,c}}$) and estimated-calculated ($e_{(z_t-z)_{e,c}}$) airgap signals.

the rail profiles are injected once the vehicle is fully laden, i.e. mass is 1250kg. Fig. 11(b) presents the deterministic airgap response to the load variation. Note that an airgap value of zero (linearised) depicts an operating point of 15mm. Clearly, with the load varying, the airgap deflection is unacceptable and well out of constraints as given in Table 2. At this point is important to note that the response in Fig. 11(b) relates to the structure shown on Fig. 5, whereby the inner loop utilizes flux measurement (without the HPF).

A practical way to avoid the large airgap deflection due to the load variation is given by the practicalities of flux sensing. In particular, we have assumed that flux is available as measurement, however in a practical situation a search coil is used [11] which provides measurement of $\frac{dB}{dt}$. Naturally, $\frac{dB}{dt}$ is integrated to provide B, although any drift in the measurement is amplified by the pure integrator. In such case, an appropriately designed High Pass Filter is used (hence, the so-called "Self-Zero Integrator" (SZI) when it is combined with the true integrator). Equation (26) presents the transfer function of the HPF $\times 1/s$, i.e.

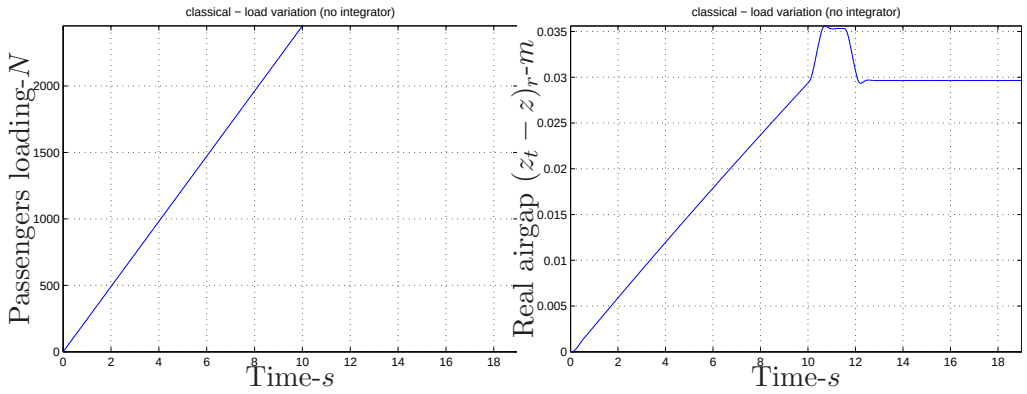

(a) *Passegers boarding profile.* **(b) *Airgap response to the passegers boarding.***

Figure 11: Passegers boarding profile and the airgap response.

characterising a butterworth type filter with cut-off frequency at 1.2rads/s with 0 deg phase shift at the given frequency. Its bode plot is shown in Fig. 12.

$$G_I = \frac{2.209s^2}{2.284s^2 + 4.7s + 4.7} \tag{26}$$

The sensitivity of the airgap to the load variations can be shown from the frequency response plot

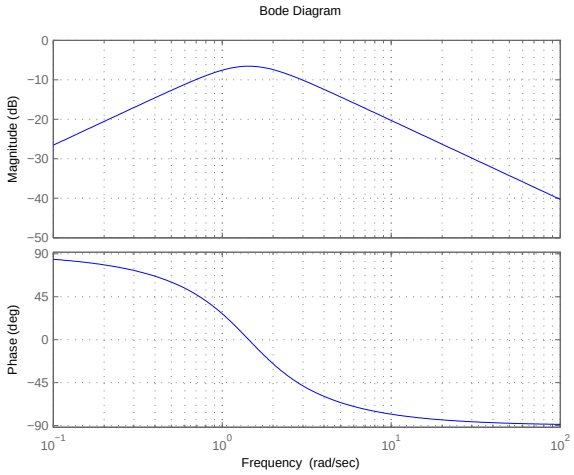

Figure 12: Frequency response of the self-zero integrator (from (26))

between $(z_t - z)$ to F_d. At the outer loop where the airgap signal is fed into the PA controller there are 4 control configurations to be studied depending on the fault scenario. For example, in the fault-free case, all feedback paths, i.e. K_e, K_c and K_m, are active in the loop. If a sensor fault happens, then the corresponding airgap signal is de-activated, while the remaining two paths are maintained active.

Figure 13 illustrates the designed system's sensitivity to F_d, i.e. frequency response from F_d to airgap, $(z_t - z)$. The frequency response without the SZI (with straight line) is flat at low frequency range while it starts dropping at around $10rad/s$. The rest of the lines are the frequency responses with a SZI in the flux density loop, this is done by inserting the HPF soon after the flux measurement as seen on the dotted line in Fig 5. With the HPF in the loop, means self-zero integration from $\frac{dB}{dt}$. Four control configurations are included, the nominal one with $K_m - K_e - K_c$ and the other three represents the sensitivity under fault conditions. The other three frequency responses are the sensitivities for the control configurations $K_m - K_e$, $K_m - K_c$ and $K_e - K_c$.

It can be seen that the attenuation is limited by adding the KE in the loop (all of the control configurations that include the KE ie. $K_m - K_e - K_c$, $K_m - K_e$ and $K_e - K_c$. It is still adequate for the normal operation of the suspension while the control configuration with $K_m - K_c$ attenuates the load disturbance in an efficient way. This can be verified from the time response of the suspension in Fig. 14(a)

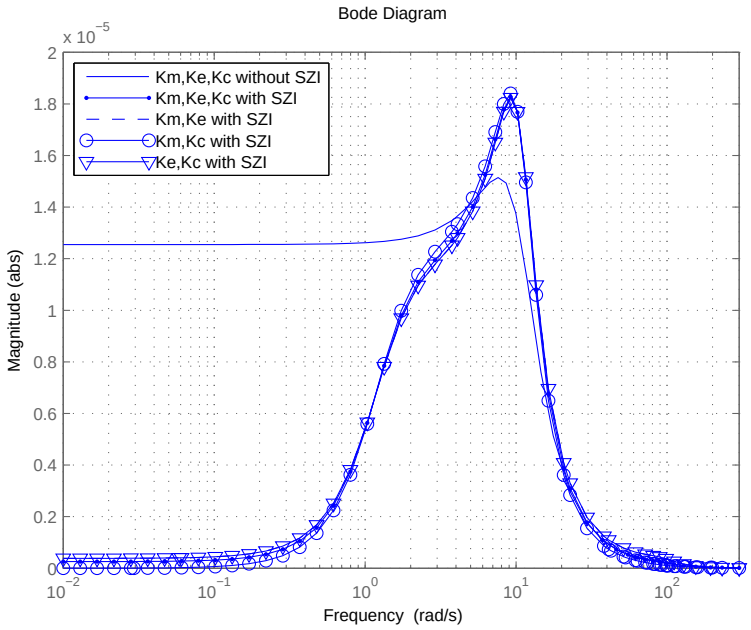

Figure 13: Frequency response between the $(z_t - z)_r$ and F_d with and without SZI in the loop.

and 14(b) where the deterministic and stochastic responses of the suspension are tested with the load variation conditions using the SZI. The responses of the airgap in both cases are characterised sufficient. The only difference is the small steady state error introduced from the KE dynamics.

5.3.2. Operating point variation

This next assessment relates to operating condition variation. It was assumed that the maglev system operates under a nominal airgap point of 15mm, however it is natural that variations of the operating condition will occur and we assume a $\pm 25\%$ variation in such case. The deterministic response of the suspension with the 4 control configurations is given in Fig. 15. Each figure shows the response in the

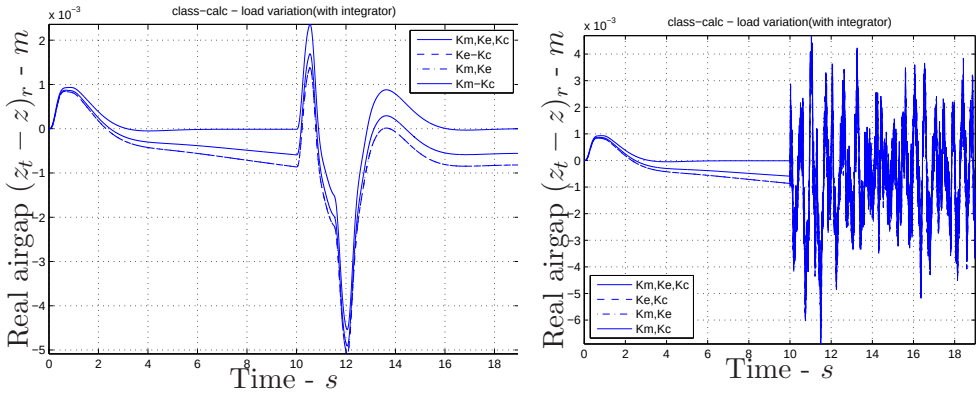

(a) *Deterministic response.* **(b) *Stochastic Responce.***

Figure 14: Closed-loop response of the suspension to disturbance inputs under load variation with SZI.

worst case perturbation of the operating point along with its nominal response (note that this includes the load variation). All of the responses show adequate performance to the worst-case perturbation with a small steady state error shown in Fig. 15(a), Fig. 15(b) and Fig. 15(d). This is expected as the sensitivity to the load variations is increased due to the use of the KE.

5.4. Sensor fault tolerance test

As it was mentioned in Section 4.1 the performance of the suspension was tested under 20 sensor fault scenarios. The performance of the suspension is illustrated on Table 3. The tests are done assuming single sensor failure at a time. Using the proposed scheme the performance of the suspension is fully recovered under any sensor faults.

Assuming that the airgap sensor (measured airgap signal) fails both fault profiles used are depicted in

Table 3: Suspension performance under various sensor fault scenarios.

	Suspension Performance under sensor fault			
	Stochastic Input		*Deterministic Input*	
Faulty sensor	Additive/abrupt fault	Multiplicative/abrupt fault	Additive/abrupt fault	Multiplicative/abrupt fault
i	✓	✓	✓	✓
b	✓	✓	✓	✓
$(z_t - z)_m$	✓	✓	✓	✓
$\dot{z}$	✓	✓	✓	✓
$\ddot{z}$	✓	✓	✓	✓

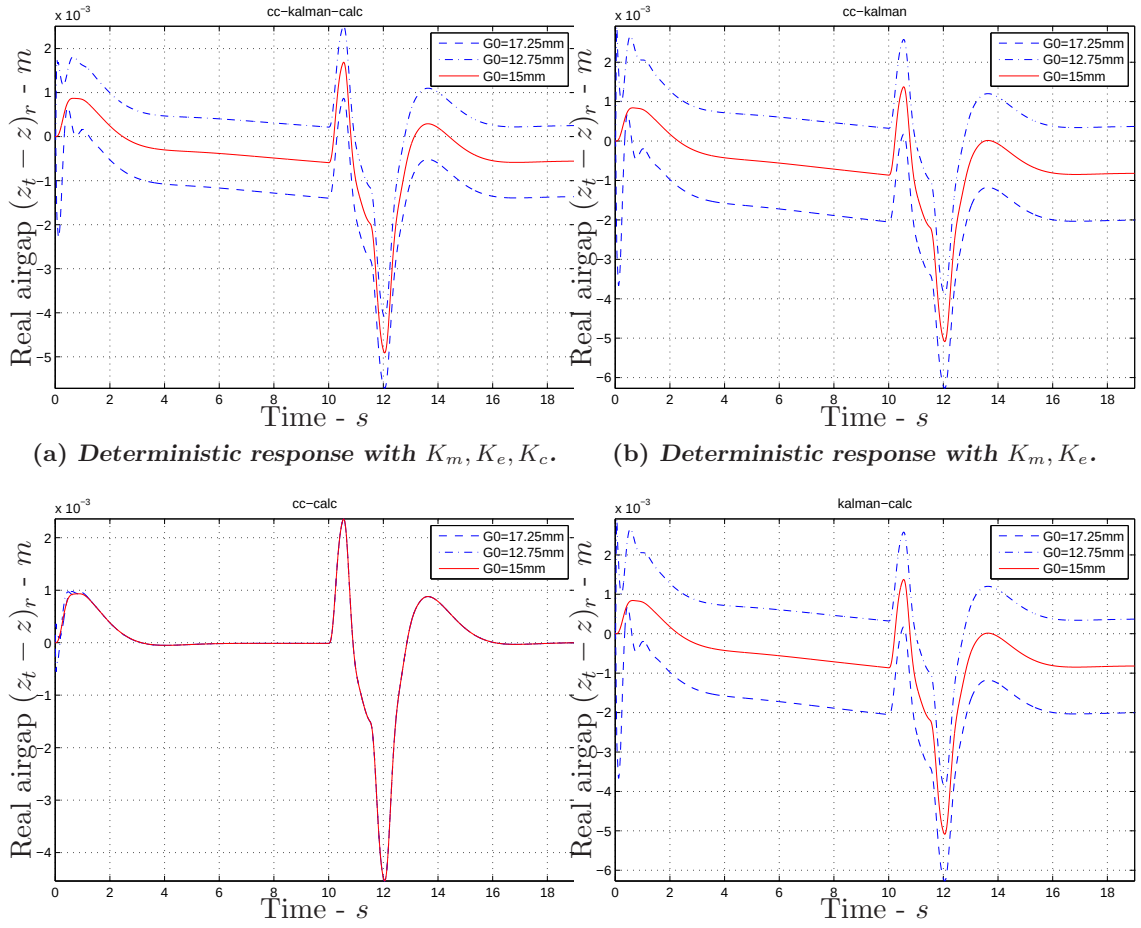

(a) ***Deterministic response with*** K_m, K_e, K_c**.** **(b)** ***Deterministic response with*** K_m, K_e**.**

(c) ***Deterministic response with*** K_m, K_c**.** **(d)** ***Deterministic response with*** K_e, K_c**.**

Figure 15: Deterministic response of the suspension with the various control configurations.

Fig 7(b) and Fig. 7(a). The error between the real airgap with fault (airgap additive/abrupt sensor fault) and fault-free conditions is depicted in Fig. 16(a). Similar response is obtained with multiplicative/abrupt fault as illustrated in Fig. 16(b). In both airgap sensor fault scenarios, the real airgap of the suspension is well within control constraints.

Linear Kalman filter techniques have proven extremely useful in engineering problems involving estimation of various quantities, one presented in this paper. However, such types of filters may suffer from convergence problems in highly nonlinear systems with large uncertainties, and this fact is acknowledged. By involving more complex estimation techniques, the complexity of the proposed solutions undoubtedly increase. However, it may be useful as a next step comparing the robustness and performance of the solutions with alternative estimation approaches, i.e. the increasingly popular Neural Networks approach [2] or finite memory filters [1].

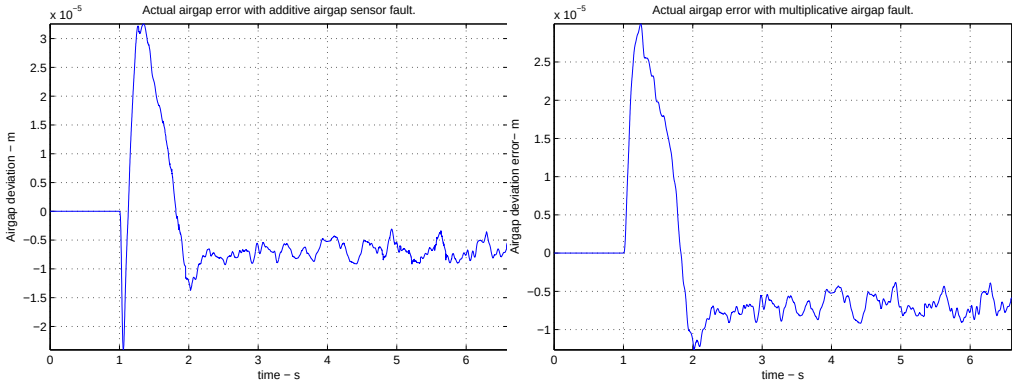

(a) $e_{(z_t-z)_{r_{f,f-f}}}$ ***with additive aigap sensor fault*** **(b)** $e_{(z_t-z)_{r_{f,f-f}}}$ ***with multiplicative aigap sensor fault.***

Figure 16: Error between the real airgap with airgap sensor fault and fault-free ($e_{(z_t-z)_{r_{f,f-f}}}$) situations.

6. Conclusions

A FTC method is presented which is used to maintain MAGLEV suspension performance under airgap sensor failure with minimum hardware redundancy and cost. Instead of having a triple or quadruple set of airgap sensors, equivalent airgap sensor information are obtained via a combination of an observer and less costly sensor elements i.e. $i, b, \dot{z}$ and $\ddot{z}$. Also, in contrast to the airgap sensor they can be installed in safer locations on the electromagnet minimizing the possibility for more faults. In addition, the proposed scheme relates to no reconfiguration of the included controller structure. Although an observer is expected to be implemented on a computer, such systems are rather common in modern train systems and are subject to appropriate computational performance. Although the inner control loop offers robustness, a drawback is the sensitivity to failures of the flux density. A current solution is that hardware redundancy may be used in the case of flux density sensor as it is a sensor providing vital information to the inner loop. Moreover, we have considered only single sensor failures in this particular study, while currently investigate solutions to simultaneous sensor failures. The proposed scheme aims to offer a first insight to control engineers working on FTC suspension systems who have to provide practical solutions but may be put off by the potential complexity of normal model-based control approaches.
Although, we have presented a MAGLEV suspension system, the scheme may be extended to more complex engineering problems. Linear Kalman Filters have proved useful in control design but they may suffer from convergence problems in the case of highly nonlinear systems with uncertainties. In this context, a particular interest in this work is extension of the framework in more robust estimators for such cases.

Acknowledgement

This work was supported in part under the EPSRC project Grant Ref.EP/D063965/1 and the Systems Engineering Innovation Centre (BAE Systems) at Loughborough University.

References

[1] C.K. Ahn. Robustness bound for receding horizon finite memory control: LyapunovKrasovskii approach. *International Journal of Control*, 85(7):942-949, 2012.

[2] C.K. Ahn and M.K. Song. $\mathcal{L}_2 - \mathcal{L}_\infty$ filtering for time-delayed switched hopfield neural networks. *International Journal of Innovative Computing, Information and Control*, 7(4):1831-1844, 2011.

[3] M. Blanke, C. W. Frei, F. Kraus, R. J. Patton, and M. Staroswiecki. What is fault-tolerant control? *Proceedings volume from the* 4^{th} *IFAC Symposium Fault Detection, Supervision and Safety for Technical Processes*, pages 40-51, 2001.

[4] C. A. C. Coello. Theoretical and numerical constraint-handling techniques used with evolutionary algorithms: A survey of the state of the art. *Computer Methods in Applied Mechanics and Engineering*, 191(11-12):1245-1287, 2002.

[5] Kalyanmoy Deb, Amrit Pratap, Sameer Agarwal, and T. Meyarivan. A fast and elitist multiobjective genetic algorithm: NSGA-II. *IEEE Transactions on Evolutionary Computation*, 6(2):182-197, 2002.

[6] P. J. Fleming and R. C. Purshouse. Evolutionary algorithms in control systems engineering: A survey. *Control Engineering Practice*, 10(11):1223-1241, 2002.

[7] B. Friedland. *Advanced Control System Design.* Prentice-Hall Inc., Upper Saddle River, NJ, USA, 1996.

[8] D. E. Goldberg. *Genetic algorithm in Search, Optimisation and Machine Learning.* Addison-Wesley Longman Publishing Co., Inc., Boston, MA, USA, 1989.

[9] R. M. Goodall. Electromagnetic suspension control without airgap measurement. *Transactions of the Institute of Measurement and Control*, 11(2):92-98, 1989.

[10] R. M. Goodall. Dynamic characteristics in the design of MAGLEV suspensions. *Proceedings of the Institution of Mechanical Engineers, Part F: Journal of Rail and Rapid Transit*, 208(1):33-41, 1994.

[11] R. M. Goodall. On the robustness of flux feedback control for electro-magnetic MAGLEV controllers. In *Proceedings of* 16^{th} *International Conference on MAGLEV Systems and Linear Drives*, pages 197-202, 2000.

[12] R. M. Goodall. Dynamics and control requirements for EMS maglev suspensions. In *Proceedings on international conference on Maglev*, pages 926-934, 2004.

[13] R. M. Goodall. Generalised design models for EMS maglev. In *Proceedings of MAGLEV 2008 - The* 20^{th} *International Conference on Magnetically Levitated Systems and Linear Drives*, 2008.

[14] J.H. Holland. *Adaptation in natural and artificial systems.* University of Michigan press, 1975.

[15] C. Huixing, L. Zhiqiang, and C. Wensen. Fault tolerant control research for high-speed maglev system with sensor failure. In 6^{th} *World Congress on Intelligent Control and Automation*, volume 1, pages 2281-2285, June 2006.

[16] Inseok Hwang, Sungwan Kim, Youdan Kim, and Chze Eng Seah. A survey of fault detection, isolation, and reconfiguration methods. *IEEE Transactions on Control Systems Technology*, 18(3):636-653, 2010.

[17] Hong-Ju Kim, Choon-Kyung Kim, and Soonman Kwon. Design of a fault-tolerant levitation controller for magnetic levitation vehicle. In *International Conference on Electrical Machines and Systems*, pages 1977-1980, October 2007.

[18] Hyung-Woo Lee, Ki-Chan Kim, and Ju Lee. Review of maglev train technologies. *IEEE Transactions on Magnetics*, 42(7):1917–1925, July 2006.

[19] Zhiqiang Long, Song Xue, Zhizhou Zhang, and Yunde Xie. A new strategy of active fault-tolerant control for suspension system of maglev train. In *IEEE International Conference on Automation and Logistics*, pages 88-92, August 2007.

[20] K. Michail. *Optimised Configuration of Sensing Elements For Control And Fault Tolerance Applied To An Electro-Magnetic Suspension System*. PhD thesis, 2009. PhD dissertation, Loughborough University, Department of Electronic and Electrical Engineering. http://hdl.handle.net/2134/5806.

[21] K. Michail, A. Zolotas, and R. Goodall. Simulation-based optimum sensor selection design for an uncertain EMS system via monte-carlo technique. In 18^{th} *IFAC World Congress*, pages 12650-12655, 2011.

[22] K. Michail, A.C. Zolotas, R.M. Goodall, and J.F. Whidborne. Optimised configuration of sensors for fault tolerant control of an electro-magnetic suspension system. *International Journal of Systems Science*, 43(10):1785-1804, October 2012.

[23] R. J. Patton. Fault-tolerant control: The 1997 situation. In *IFAC Symposium on Fault Detection Supervision and Safety for Technical Processes*, volume 3, pages 1029-1052, 1997.

[24] M. G. Pollard. MAGLEV - a british first at birmingham. *The Institute of Physics*, 15:61-72, 1984.

[25] S. Skogestad and I. Postlethwaite. *Multivariable Feedback Control Analysis and Design*. John Wiley & Sons Ltd, 2^{nd} Edition, New York, 2005.

[26] H. K. Sung, S. H. Lee, and Z. Bien. Design and implementation of a fault tolerant controller for EMS systems. *Mechatronics,*, 15(10):1253-1272, 2005.

[27] N. Eva Wu, Sudha Thavamani, Youmin Zhang, and Mogens Blanke. Sensor fault masking of a ship propulsion system. *Control Engineering Practice*, 14(11):1337-1345, 2006.

[28] Song Xue, Zhiqiang Long, Guang He, and Ning He. Sensor fault diagnosis of maglev train based on kalman filter group. In 5^{th} *International Conference on Intelligent Computation Technology and Automation*, pages 312-316, January 2012.

[29] Youmin Zhang and Jin Jiang. Bibliographical review on reconfigurable fault-tolerant control systems. *Annual Reviews in Control*, 32(2):229-252, 2008.

[30] Zhizhou Zhang, Zhiqiang Long, Longhua She, and Wensen Chang. Fault-tolerant control for maglev suspension system based on simultaneous stabilization. In *IEEE International Conference on Automation and Logistics*, pages 299-303, August 2007.

[31] Zhizhou Zhang, Lingling Zhang, and Zhiqiang Long. Active fault tolerant control for maglev train against accelerometer failure. In *IEEE International Conference on Robotics and Biomimetics*, pages 1356-1360, 2009.